# Disentangling the Factors of Convergence between Brains and Computer Vision Models

Joséphine Raugel[1,2], **Marc Szafraniec**[1], **Huy V. Vo**[1], **Camille Couprie**[1], **Patrick Labatut**[1], **Piotr Bojanowski**[1], **Valentin Wyart**[2], **Jean-Rémi King**[1]

[1]Meta AI, [2]Ecole Normale Supérieure - PSL Université

Many AI models trained on natural images develop representations that resemble those of the human brain. However, the exact factors that drive this brain-model similarity remain poorly understood. In order to disentangle how the model architecture, training recipe and data type independently lead a neural network to develop brain-like representations, we trained a family of self-supervised vision transformers (DINOv3) that systematically varied these different factors. We compare their representations of natural images to those of the human brain recorded with both ultra-high field functional magnetic resonance imaging (fMRI) and magneto-encephalography (MEG), providing high resolution in spatial and temporal analyses. We assess the brain-model similarity with three complementary metrics focusing on overall representational similarity, topographical organization, and temporal dynamics. We show that all three factors – model size, training amount, and image type – independently and interactively impact each of these brain similarity metrics. In particular, the largest DINOv3 models trained with the largest amount of human-centric images reach the highest brain-similarity scores. Importantly, this emergence of brain-like representations in AI models follows a specific chronology during training: models first align with the early representations of the sensory cortices, and only align with the late and prefrontal representations of the brain with considerably more training data. Finally, this developmental trajectory is indexed by both structural and functional properties of the human cortex: the representations that are acquired last by the models specifically align with the cortical areas with the largest developmental expansion, the largest thickness, the least myelination, and the slowest timescales. Overall, these findings disentangle the interplay between architecture and experience in shaping how artificial neural networks come to see the world as humans do, thus offering a promising framework to understand how the human brain comes to represent its visual world.

Correspondence: {josephiner,jeanremi}@meta.com

∞ Meta
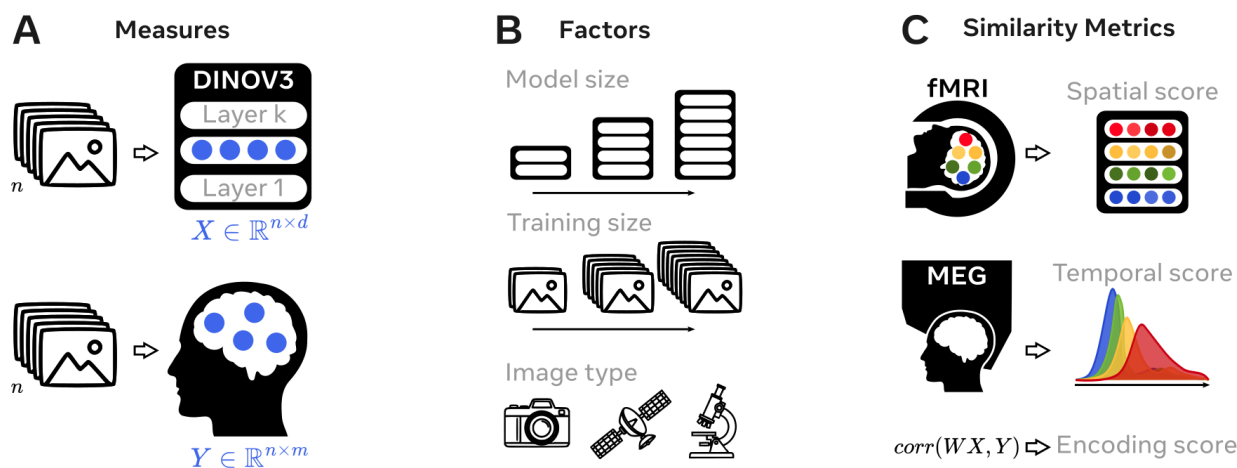
A. We compare the activation of DINOv3, a state-of-the-art self-supervised computer vision model trained on natural images, to the activations of the human brain in response to the same images. **B.** To understand the factors that make DINOv3 more-or-less similar to the brain, we train *from scratch* a variety of models on different image domains (pictures from human-centric cameras, satellite images or biological data), and with a varying amount of data. **C.** We compare each model to both functional Magnetic Resonance Imaging (fMRI, with high spatial resolution) and Magneto-Encephalography (MEG, with high temporal resolution) by computing the overall linear similarity of their representations (encoding score) and the similarity of their hierarchical organization (spatial and temporal scores).

1 Introduction

Brain-AI similarity. Deep learning has transformed computer vision over the past decade. State-of-the-art deepnets now achieve human-level or superior performance across a variety of tasks including classification (Siméoni et al., 2025; Tschannen et al., 2025), object detection (Redmon et al., 2016), semantic segmentation (Cheng et al., 2022), and medical image analysis (Esteva et al., 2017; Lorenci et al., 2025).

Surprisingly, the internal representations of these deep learning models appear to be related to those of the human brain: multiple electrophysiology (Yamins et al., 2014a; Yamins and DiCarlo, 2016; Schrimpf et al., 2018; Zhuang et al., 2021), functional Magnetic Resonance Imaging (Eickenberg et al., 2017; Millet et al., 2023; Doerig et al., 2025; Tang et al., 2023; Nikolaus et al., 2024), magneto-encephalography studies (Cichy et al., 2016; Seeliger et al., 2018; Caucheteux and King, 2022; Banville et al., 2025) have now consistently shown that the activation patterns of these models linearly map onto those of the cortex in response to the same images.

Theoretical importance. Understanding the principles at the origin of this representational similarity between AI models and the human brain is of primary importance, to understand the laws of information processing that may be universally shared across neural networks. Indeed, several lines of research (Hasson et al., 2020; Huh et al., 2024; van Rossem and Saxe, 2024; Cagnetta et al., 2024; Mehrer et al., 2020; Mahner et al., 2025; Simkova et al., 2025) suggest that there exists universal principles that constrain the structure and emergence of representations in neural networks.

Challenge: Unclear causes. However, the precise factors responsible for the representational similarity between computer vision models and the human remain currently unclear. This gap of knowledge is partly due to the fact that previous studies primarily focused on pretrained networks, that *simultaneously* vary in training objectives, architectures and data regime (Conwell et al., 2021; Rajesh et al., 2024). How each of these factors independently and interactively lead a model to converge to brain-like representations thus remains unclear.

To address this issue, we systematically train a variety of DINOv3 models (Siméoni et al., 2025), while independently varying their size, data type and training quantity. DINOv3 has the advantage of being self supervised, and can thus be trained on different types of naturalistic but non-human centric and non-labelled data such as satellite images (Siméoni et al., 2025) and biological images (Lorenci et al., 2025).

Here, we compare a variety of DINOv3 models to the brain responses to images, as recorded with ultra high field (7T) functional MRI and magneto-encephalography (MEG) to get a high spatial and temporal resolution of the cortical representations, respectively. For this, we implement three similarity metrics. First, we use a standard linear mapping metric, often referred to as *encoding score* (Naselaris et al., 2011), which evaluates the linear correspondence between the representations of two systems. Second, we evaluate, with fMRI, whether this linear mapping follows a similar *spatial* organization, whereby the first and last layers of the model would best match the sensory visual and prefrontal cortices, respectively. Finally we evaluate, with MEG, whether this mapping follows a similar *temporal* organization, whereby the first and last layers of the model best match the early and late MEG responses, respectively.

2 Method

2.1 Approach

We aim to identify the factors that make modern computer vision models process and represent natural images similarly to the human brain. Following previous work (Kriegeskorte et al., 2008; DiCarlo et al., 2012; King and Dehaene, 2014), we rely on the definition of "representation" as "linearly readable information". We employ the encoding analysis procedure introduced by Naselaris et al. (2011) to evaluate the representational similarity between an AI model and brain recordings. This linear model seeks to find whether there exists a linear mapping $W \in \mathbb{R}^{m \times d}$ that reliably predicts m-dimensional brain activity ($Y \in \mathbb{R}^{n \times m}$) given the d-dimensional model activation ($X \in \mathbb{R}^{n \times d}$) in response to n images:

$$\underset{W}{\arg\min} \left\{ \|Y - XW\|_2^2 + \lambda \|W\|_2^2 \right\}$$

with λ the ridge regularization parameter.

For this, we use scikit-learn's `RidgeCV` (Pedregosa et al., 2011) and 10 logarithmically-spaced regularization λ in between 10^0 and 10^8, and a 5-split cross-validation.

2.2 Metrics

Encoding score   Given two representations X and Y, we quantify their overall representational similarity by computing, for each split separately and then averaged, an *encoding score* with a Pearson correlation score $R \in [-1, 1]$:

$$R^{(d)} = corr(WX_{test}, y_{test}^{(d)})$$

For clarity, we can either summarize the average R score across brain dimensions, or plot them all separately to get information about where brain activations are linearly predictable from the model. In some analysis, we use $\tilde{R} = R/max(R)$, the normalized encoding score, which peaks at 1.

Spatial score   To assess whether a model organized its processing hierarchy similar to that of a brain with a *spatial score*, we proceed in four steps. First, we evaluate an encoding score for each dimension d of the brain, and from 22 layers $k \in [0, 1]$ of the model, where 0 is the first layer, and 1 is the last layer. Second, we identify the layer that best predicts this brain response: k^*. Third, we approximate the hierarchical position d^* of each brain region, as its Euclidean distance from V1 in the standardized MNI space, in mm. Note that this is a coarse approximation, as the actual cortical hierarchy does not strictly follow such distances, and may be considerably more complex (Felleman and Van Essen, 1991). Finally, we compute the spatial score as the correlation between d^* and k^*. For clarity we restrict these analyses to regions of interest.

Temporal score   To evaluate an analogous metrics from MEG recordings, we estimate a *temporal score*: i.e. the correlation between the model layers k and t^* – the time at which each layer of the model is maximally predictive of brain activity. To limit noisy estimate, we average of the temporal window during which $\tilde{R}^k \geq 95\%$ where $\tilde{R}^k$ is the normalized brain-score of the layer k.

2.3 Models

Architecture.   DINOv3 is a state-of-the-art self supervised learning vision transformer model trained on 1.7 billion natural images (Siméoni et al., 2025). We train, from scratch, a selection of eight variants of this DINOv3 model to ensure a comprehensive evaluation ranging through architectures, training scale and data types.

First, we leverage the DINOv3-7B, trained across $1e^7$ checkpoints. We analyze comparatively DINO Small,

Base, Large and Giant, after training for $5e^6$ training steps on 1.7B images with the same configuration. Additionally, we train and analyze comparatively 3 versions of the DINO Large architecture: DINO Human, DINO Cellular and DINO Satellite. These models were configured similarly and trained, from scratch, over $5e^6$ steps on 10M images; they only differ in the type of images with which they were trained.

2.4 Datasets.

Images.   DINOv3-7B and Dino Human were trained on the same human-centric data. This dataset was constructed from a large pool of web images obtained from public Instagram posts, street views and ImageNet (Deng et al., 2009). These images went through platform-level content moderation to prevent harmful contents, in order to obtain an data pool of approximately 17 billion images. This data pool was curated following the procedure in (Siméoni et al., 2025) to obtain a large-scale pre-training dataset of 1.7 billion images. To compare models trained with different types of images, we re-trained three distinct large DINOv3 with one of three types of natural images – human-centric, cellular and satellite images – matched in terms of quantity (10M images each).

Human-centric images correspond to the dataset used for training the original DINOv3 model. For our comparative analyses on human-centric, cellular and satellite images, we randomly selected from this dataset of 1.7 billion images a subset of 10 million images.

Cellular images correspond to the ExtendedCHAMMI dataset, which consists of fluorescent microscopic images of cells revealing cellular structures into different channels (e.g. nucleus, mitochondria, microtubules, etc.) (Lorenci et al., 2025).

Satellite images correspond to a random subset of the SAT-493M dataset, which consists of approximately 500 million sampled randomly from Maxar RGB ortho-rectified imagery at 0.6 meter resolution (Siméoni et al., 2025).

Magnetoencephalography (MEG).   We use the THINGS-MEG dataset (Hebart et al., 2023a), which consists of MEG recordings from four healthy participants viewing 22,500 naturalistic images, representing a total of 1,800 object concepts (Hebart et al., 2023b). Images were presented during 1.5 s, while participants maintained fixation. To limit the impact of noise we apply a bandpass filter between 0.1 and 20 Hz, down-sample the signal at 30 Hz, time-lock the brain responses to individual words, and epoch the

Model	Parameters	Layers	Batch Size	Images
DINOv3	7B	40	4096	Human centric 1.7B
DINOv3 Giant	1.1B	32	4096	Human centric 1.7B
DINOv3 Large	300M	24	4096	Human centric 1.7B
DINOv3 Base	86M	12	4096	Human centric 1.7B
DINOv3 Small	21M	12	4096	Human centric 1.7B
DINOv3 Human	300M	24	2048	Human centric 10M
DINOv3 Cellular	300M	24	2048	Cellular 10M
DINOv3 Satellite	300M	24	2048	Satellite 10M

Table 1 Specifications of DINOv3 model variants.

corresponding neural data between -0.5 s and +3 s relative to word onset using MNE-Python (Gramfort et al., 2013). Finally, we z-score MEG signals across words, for each MEG channel and each time point independently.

time ROIs. We study individually three 5s-long time ROIs across the processing time of an image, to study the relative impact of each layer in the encoding of the cognitive process at play during that time. These time windows span .08-.13s, .13-.18s and .5-.55s.

T_{max}^{layer}. To study the dynamics of each layer, we compute $T_{\max}^{layer}$, the mean of the temporal window during which $\tilde{R}^{layer} \geq 95\%$ where $\tilde{R}^{layer}$ is the normalized brain-score of each layer.

Functional Magnetic Resonance Imaging (fMRI). We leverage the Natural Scenes Dataset (Allen et al., 2022), a 7 tesla fMRI dataset which consists of recordings from eight subjects, each observing a total of 10 000 natural scenes during 4 seconds each, while performing a continuous recognition task. We encode the BOLD signal on the fsaverage surface at 5.5 s after image onset. This timestep corresponds to the peak of decoding of the image from the BOLD signal.

Regions of interest (ROIs). For clarity, we select a representative set of 15 regions of interest (ROIs) spanning the anatomy of the cortex, among the regions encoded with an averaged FDR-corrected t-test $p < 0.01$, among voxels forming the ROI). These ROIs are distributed from posterior-occipital lobe to prefrontal cortex. To investigate the cortical properties that index representational similarity, we analyze our results in light of four cortical maps, made available through Neuromaps (Markello et al., 2022):

Cortical expansion (Hill et al., 2010) reflects the difference of cortical surface area between infants and adults.

Myelin concentration is estimated from the T1w/T2w ratio in the HCP S1200 dataset (Van Essen et al., 2013).

Intrinsic timescales are derived from mapping electromagnetic networks (measured through MEG) to

hemodynamic network (measured through fMRI) and indexing the temporal integration window of each region (Shafiei et al., 2021).

Cortical thickness is estimated by measuring the distance between "white" and "pial" Freesurfer (Fischl, 2012) surfaces from structural MRI in the Human Connectome Project (Van Essen et al., 2013).

2.5 Statistics

fMRI voxels. We only plot and analyze voxels thresholded with $p < 0.01$ after a FDR-corrected t-test.

Across subjects. To evaluate statistical estimates across subjects, we perform a Wilcoxon test using scipy (Virtanen et al., 2020). To correct for multiple comparison, we apply a false discovery rate correction, as implemented in MNE-Python (Gramfort et al., 2013).

Half times. To analyze the speed of convergence of DINO models during training, we estimate the 'half time': the relative training step at which the similarity metric reaches half of its final value.

3 Results

3.1 DINOv3-brain similarity

Encoding score. To verify that DINOv3 generates representations of natural images that are similar to those of the brain, we perform a cross-validated encoding analysis by evaluating the linear mapping between the activations of DINOv3 and of the brain in response to the same images. Functional MRI results show that DINOv3 has representations that primarily peak in the visual pathway (R=.45 ± .039 - SEM across subjects), mostly in the lateral-occipitotemporal (MT: R=.34±.026) and ventromedial visual cortex (VMV2: R=.28 ± .025), Fig 2A.

MEG results show that this similarity rises around 70 ms after image onset (R=.09 ± .017, Fig 2B) and re-
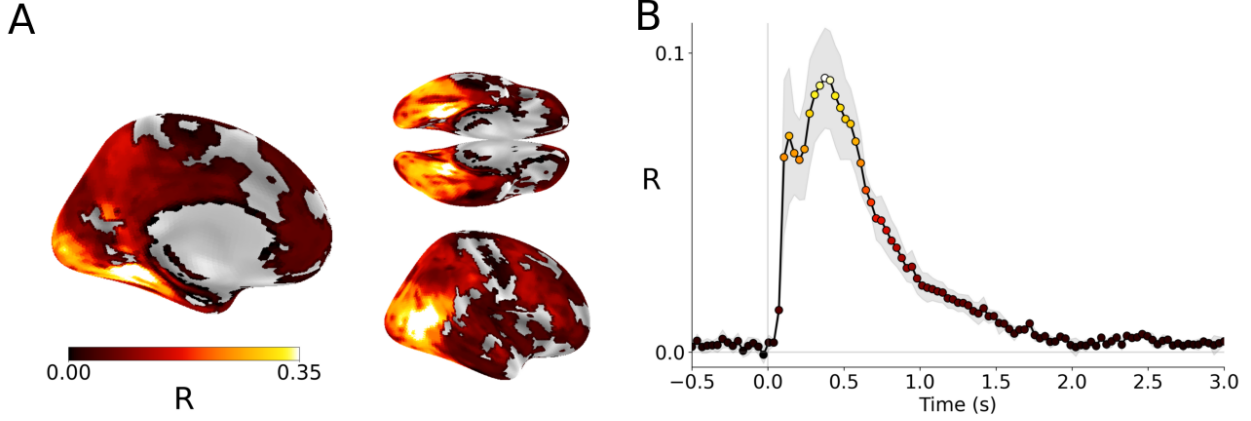
Figure 2 Brain-DINOv3 similarity. A. Similarity between DINOv3 embedding and the fMRI responses to corresponding images as estimated with a Pearson Brain-Score, and fdr-corrected-thresholded at p < 0.01 (left: medial view of left hemisphere, top right: bottom view; bottom right: lateral view of right hemisphere). **B.** Similarity between DINOv3 embedding and MEG responses to the corresponding images. The error bar indicates the standard error of the mean across 4 subjects watching still images.

mains significantly above chance level up to 3 seconds after image onset (p < 1e-3).

These results are consistent with past studies (Eickenberg et al., 2017; Schrimpf et al., 2018; Tang et al., 2025) and additionally show that areas typically discarded from the visual pathways, e.g. prefrontal regions BA 44, BA 45, IFSa and IFSp, also present activations that are linearly predictable from the AI embedding.

Spatial score. Does the hierarchy of representations of DINOv3 correspond to the visual hierarchy in the human brain? To address this question, we estimate the "spatial score". The fMRI results confirm that the lowest layers of DINOv3 tend to best predict the lower-level sensory regions such as V1, whereas the highest layers tend to best predict higher-level regions of the brain, such as the prefrontal cortex (Fig 3A, C, E). A Pearson correlation between (i) the Euclidean distance between each brain region and V1, and (ii) the best encoding layer is highly significant, R=0.38, p < $1e^{-6}$ (Fig 3E).

Temporal score. To complement this fMRI "spatial score", we evaluate an MEG "temporal score". For this, we identify the layer which best predicts each time ROIs relative to image onset in the MEG (Fig 3B). The results show a significant correlation between $T_{\max}^{layer}$ and layers, hereafter referred to as the temporal score (Fig 3B, D, F). The temporal score R=0.96, p< $1e^{-12}$, shows that the first and last layers of DINOv3 consistently align with the earliest and

latest MEG responses, respectively.

3.2 What factors lead DINOv3 to become brain-like?

Impact of training. To clarify the emergence of brain-like processes in DINOv3, we evaluate the encoding score, spatial score and temporal score at each selected training step of DINOv3, and then summarize their developmental speed with a "half time": i.e. the training step where half of the final score is reached.

First, before training the encoding score reaches R=.03 ± $2e^{-4}$, after training it ultimately converges to R=.09 ± $5e^{-4}$. These R-scores are averaged across voxels – the best voxel peaking at R=.45 ± .038(Fig 4A, B, E). The half time of the encoding score occurs around 2% of the training, around 10^5 training steps (i.e. 800 million images). Second, the temporal scores emerge faster than brain-scores: with a half time around 0.7% of the training, and a convergence at R=0.96 (p< $1e^{-12}$). Finally, the spatial score reaches its half time at 4% of the training and converges to R=0.4 (p< $1e^{-6}$). Are these developmental trajectories identical across temporal and brain regions of interest ? To address this issue, we evaluate the same analyses on specific regions or temporal windows of interest. Functional MRI results show that low-level visual regions (e.g. V1, V2) are marked by lower half times than high-level prefrontal cortices (e.g. IFSp, IFSa; Fig 5A,C). The correlation between half time and anatomical location (coarsely defined as the Euclidean distance to V1) is R=0.91, p< $1e^{-5}$. Sim-
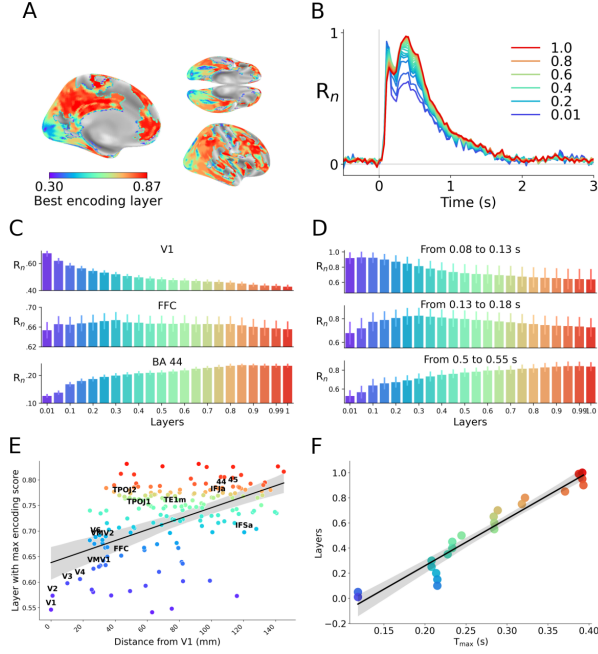
Figure 3 The representational hierarchy of DINOv3 corresponds to the brain's A. Voxel-wise best encoding layers of DINOv3, FDR-corrected and thresholded at p < 0.01 (left: medial view of left hemisphere, top right: bottom view; bottom right: lateral view of right hemisphere). **B.** Dynamic brain-score across time between each layer of DINOv3 and MEG responses to the corresponding still images. **C.** Scaled brain-scores across layers for three regions of interest across the cortex: V1 (up), Fusiform Face Cortex (middle) and Broadmann 44 (down). Encoding scores scores are scaled for each layer, by the maximal encoding score of this layer among the 15 studied ROIs. **D.** Scaled brain-scores across layers for three time windows of interest during the processing of an image: .08-.12s (up), .13-.18s (middle) and .5-.55s (down). Encoding scores are scaled for each layer, by the maximal encoding score of this layer across time. **E.** Plotting the correlation between the best encoding layer for each region and the euclidean distance of this region from V1, in mm. The Pearson correlation is r = 0.38, p < 1e-6. Plotted regions are encoded with FDR-corrected thresholding at p < 0.01. **F.** Plotting the correlation between the best encoding layer for each timestep and the $T_{\max}^{layer}$, in s. The Pearson correlation is r = 0.84, p < 1e-5. Plotted regions are encoded with FDR-corrected thresholding at p < 0.01.

ilarly for MEG, earlier windows (e.g. <200 ms) are marked by lower half times than late time windows (e.g. >1,500 ms; Fig 5B,D). The correlation between half time and temporal peak is R=0.84, p< $1e^{-5}$. Overall, these results show that the brain responses of the sensory and prefrontal cortices contain representations of images that are acquired relatively early and late in the training of DINOv3, respectively.

Impact of model size. Dino models of larger scale appear to converge quicker and encode higher-level ROIs more accurately. How does model size impact convergence? Model size consistently leads to bigger encoding scores at the end of training ($R_{\text{Giant}} = 0.107 > R_{\text{Large}} = 0.105 > R_{\text{Base}} = 0.101 > R_{\text{Small}} = 0.096$ with p < $1e^{-3}$), Fig 6B). Similar, although noisier phenomena can be observed for spatial scores and temporal scores (p < $1e^{-3}$), Fig 6A, B.

Does model size impact encoding scores similarly across ROIs? Applying the same analysis for each ROI separately (Fig 6C, D) shows that model size primarily increases encoding of higher-level cortices like BA44 and IFS as compared to visual cortices like V1, V2. All models present this size-dependent increased encoding significantly in higher-ROIs, only the smallest ones in V1, V2 (p < $1e^{-3}$), Fig 6C, D.

Impact of image type. To assess how image types influence the development of brain-like representations in a model, we trained, from scratch, three distinct DINO models, each using one of three natural images datasets: satellite images, cell images and classic (human-centric) images. We focus on a single DINOv3 architecture (Dino Large), with a fixed training length and training data quantity (10M images) and have data type as the only varying factor. Training improves encoding scores, spatial scores and temporal scores for all image types (Fig 7A), suggesting that these models learn visual features that are universal across these different types of natural images. However, these brain-similarity metrics are lower for satellite and cell images than for human centric images, for encoding, spatial and temporal scores. Interestingly, this difference is observed across most regions of interest: e.g. both V1 (p < $1e^{-3}$) and IFSa (p < $1e^{-3}$) are better encoded by a model trained with human centric photos than other models. At the end of training, Dino Human reaches a significantly higher performance regarding brain-score, temporal and spatial scores (p < $1e^{-3}$), Fig 7B. These results might unravel from the fact that human centric images reflect visual input that brains are exposed to, whereas satellite images and cell images are images that brains have not been trained to process.

3.3 Link to cortical properties

Is the development of brain-like representations predicted by functional, structural and developmental properties of the cortex? To explore this issue, we evaluate the correlation between the representational half time of encoding and four properties of the cortex.
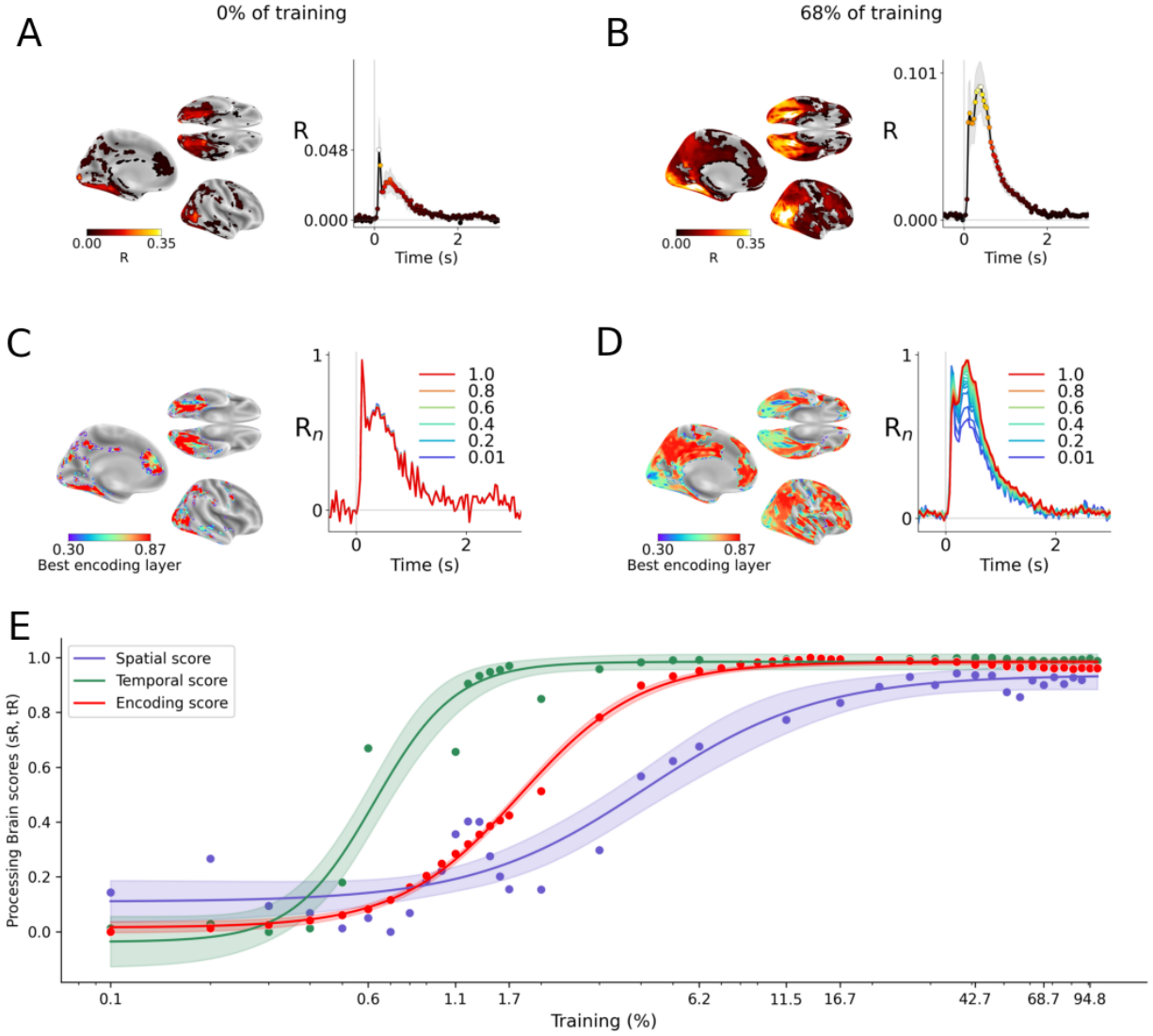
Figure 4 A. fMRI and MEG encoding scores from an untrained DINOv3. **B.** Encoding scores for a DINOv3 trained at 68% of its training. **C.** Scores for an untrained DINOv3. Left. Best encoding layer for each voxel of each fMRI ROI. Right. Relative encoding score for 10 representative layers of an untrained DINOv3 (0=first layer, 1=last layer). **D.** Same as C for a DINOv3 trained at 68% of its training. **E.** Evolution of temporal, encoding and spatial scores as a function of DINOv3's training.
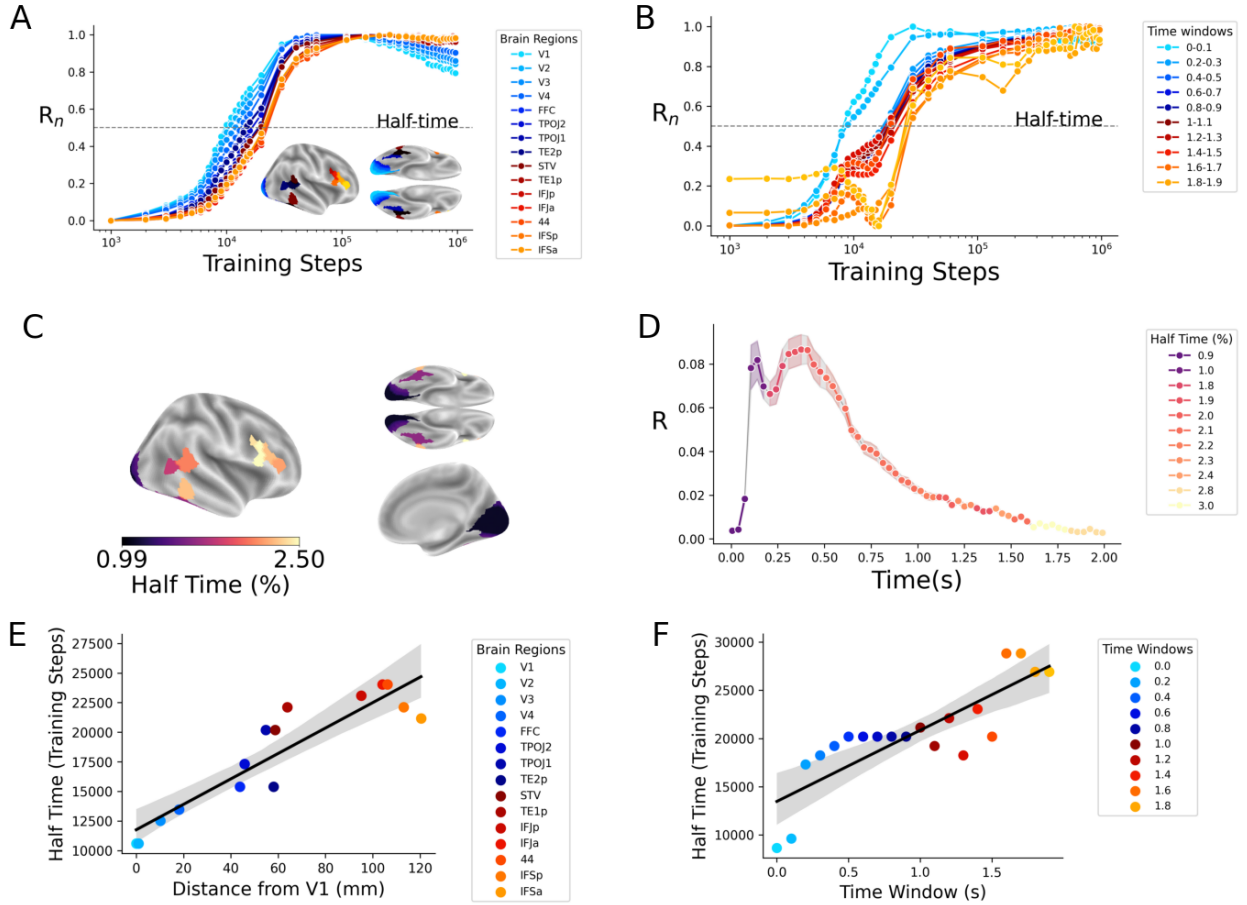
Figure 5 Emergence of brain-like representations. **A.** Normalized brain encoding scores as a function of training for each brain ROI. The dashed line indicates the 50% of the maximum encoding score for each region. **B.** Same as A for MEG time region of interest. **C.** Half time for each brain region of interest. **D.** Half time for each time region of interest. **E.** Correlation between half time of encoding score across training, and distance of each ROI from V1. **F.** Correlation between half time of encoding score across training, and time position of the encoded cognitive process.
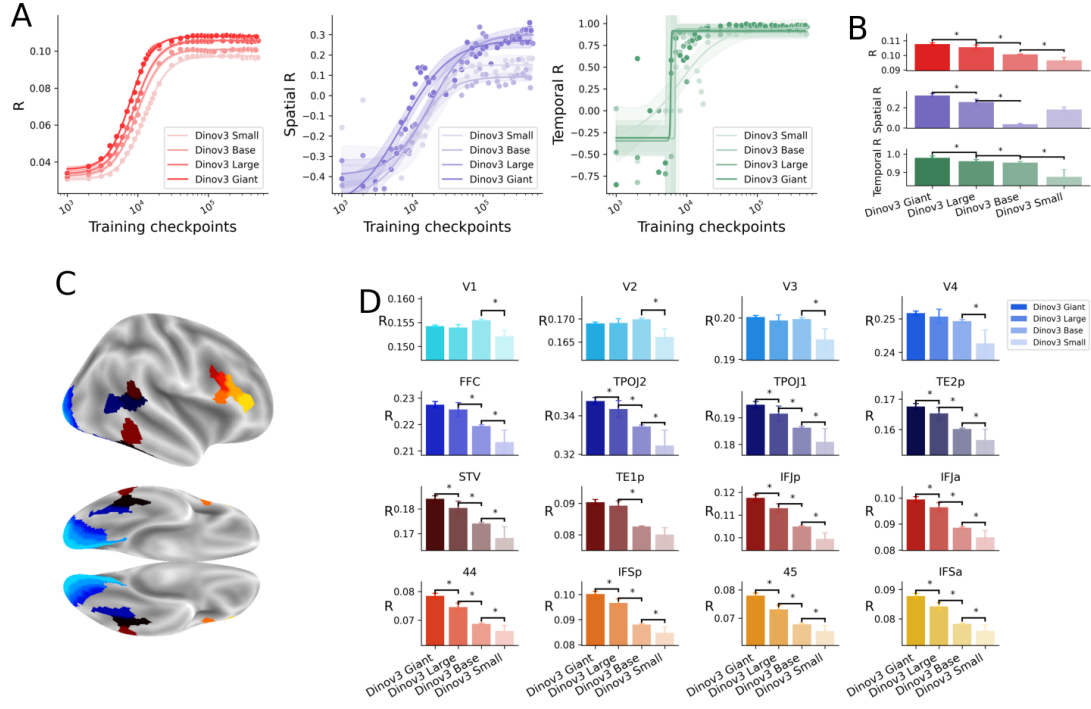
Figure 6 Impact of model size. For inter-model comparisons, significance to p<$1e^{-3}$ are represented by asterisks *. **A.** Encoding (reds), spatial (purples), and temporal scores (greens) as a function of training and model size. Logarithmic fits of scores across training. **B.** Scores on the final k=$4e^5$ training steps. **C.** Brain ROIs. **D.** Encoding scores for each ROI at the end of training.
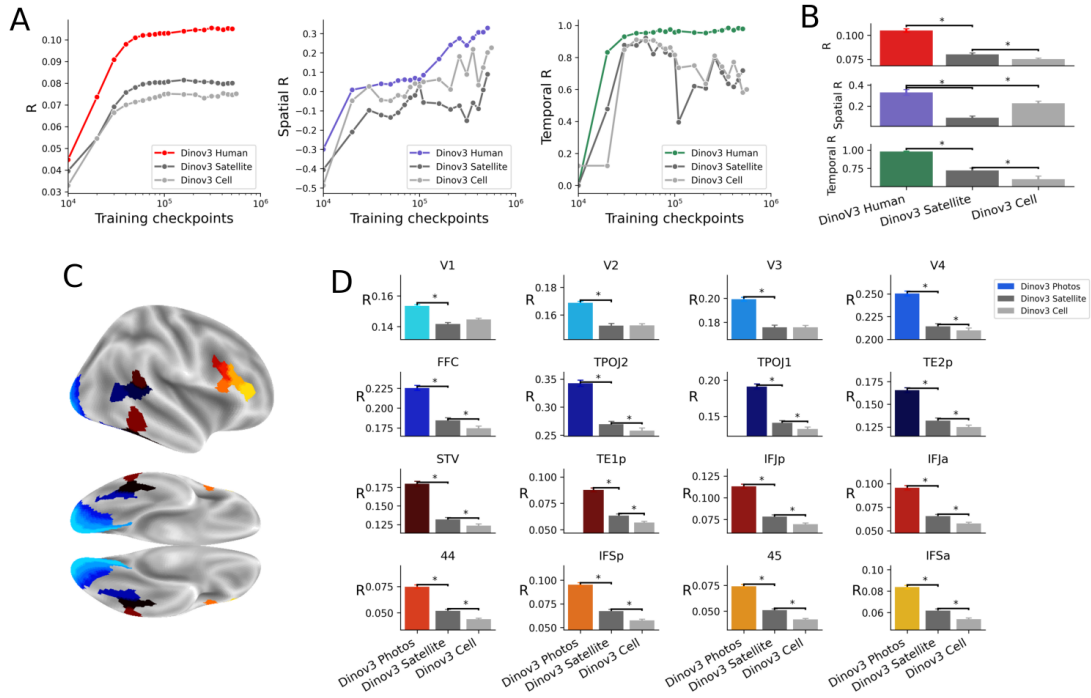
Figure 7 Impact of image type. For inter-model comparisons, significance to p<$1e^{-3}$ are represented by asterisks *. **A.** Encoding (reds), spatial (purples), and temporal scores (greens) as a function of training and image type. **B.** Scores on the final k=$4e^5$ training steps. **C.** Brain ROIs. **D.** Encoding scores for each ROI at the end of training.

Cortical expansion. First, we focus on the developmental expansion of cortical regions. Using an atlas comparing infant and adult cortical structures (Hill et al., 2010), we found a strong positive correlation (R=0.88, p $< 1e^{-3}$) between half time and cortical expansion (Fig 8A). This indicates that cortical areas marked by greater developmental growth are also those whose representations emerge later in the AI model.

Cortical thickness. Second, we assess the correspondence with cortical thickness, utilizing HCP S12000 estimates. Our results show a significant correlation (R=0.77, p $< 1e^{-2}$), suggesting that cortical areas with larger cortical sheets exhibit longer half times (Fig 8B).

Cortical dynamics. Third, the areas with the slowest intrinsic dynamics, as estimated from a source-reconstruction of MEG activity, are also those that tend to have the longest half times (R=0.71, p = .022). This result directly echoes our MEG results (Fig 5), whereby deeper layers of DINOv3 tend to be associated with slower brain responses (Fig 8C).

Cortical myelin. Finally, this dynamic property appears linked to myelin concentration (Van Essen et al., 2013). Myelin, which facilitates faster neuronal transmission, demonstrated a strong negative correlation with half time (R=-0.85, p-val $=1e^{-3}$). This implies that higher myelin concentration is associated with shorter half times (Fig 8D).

In summary, these findings demonstrate a strong predictive relationship between the speed at which brain-like representations emerge in AI models and various structural and functional characteristics of the cortex, across development and once developed.

4 Discussion

Main findings. Understanding why artificial neural networks develop representations that resemble those in the human brain remains a fundamental challenge to neuroscience and AI (Huh et al., 2024; Hasson et al., 2020; Shen et al., 2025; Caucheteux and King, 2022). While recent studies have documented brain–model similarities across a wide range of architectures and training paradigms (Conwell et al., 2022), the exact factors that cause this convergence remain unclear. Here, we independently manipulate three independent factors – model size (from DINOv3 small to giant), training length (from 0 to $1e^7$ steps on several training sets of 10M and of 1.7B images) and image type (human-centric, satellite images and biological images) to test how each of them contributes to the emergence of brain-like representations of natural images. Our findings demonstrate that these three factors all independently and interactively impact the extent to which a self supervised model converges to brain-like visual processing.

Nativism and empiricism. In particular, the model–brain similarity increases consistently with larger architectures, longer training, and more ecologically valid data. These results are consistent with an increasing set of studies showing linearly aligned representations of natural images (Yamins et al., 2014b; Kriegeskorte, 2015; Schrimpf et al., 2018; Tang et al., 2025; Thobani et al., 2025), with a hierarchy that maps the functional organization of the visual cortices (Eickenberg et al., 2017; La Tour et al., 2022), and dynamics that reflect the ordering of the model's layers (Seeliger et al., 2018; Cichy et al., 2016; Caucheteux and King, 2022).

In addition to its factorial disentanglement, our study provides additional contributions.
First, this model-brain alignment is not confined to the visual pathways (Eickenberg et al., 2017; Schrimpf et al., 2018; Tang et al., 2025) but extends into high-level – multi-modal – regions of the cortex, including the prefrontal cortex (although see e.g. Solomon et al. (2024) for a low-dimensional set of image features identified in the prefrontal lobe).
Second, our independent manipulation of model size, training duration, and data type further show how these factors *interact* with one another: the largest architectures best align with brain activity as (1) they get trained and (2) on ecologically-relevant naturalistic images.
Third, even non-human-centric datasets (satellite images, biological images) support partial convergence in early visual areas, implying that low-level statistics shared across environments are sufficient to bootstrap early representations. Overall, these results suggest that while the architecture supplies a potential, the data remain critical in making these systems learn representations that are similar to the brain. This interaction between architectures, training and data provides an empirical framework to the long-standing debates in cognitive science on nativism versus empiricism, – showing how 'innate' and 'experiential' interact with one another in the development of cognition.

Towards a model of the visual cortex ontogeny. This model-brain alignment follows a surprisingly steady developmental trajectory. Early in training, the mod-
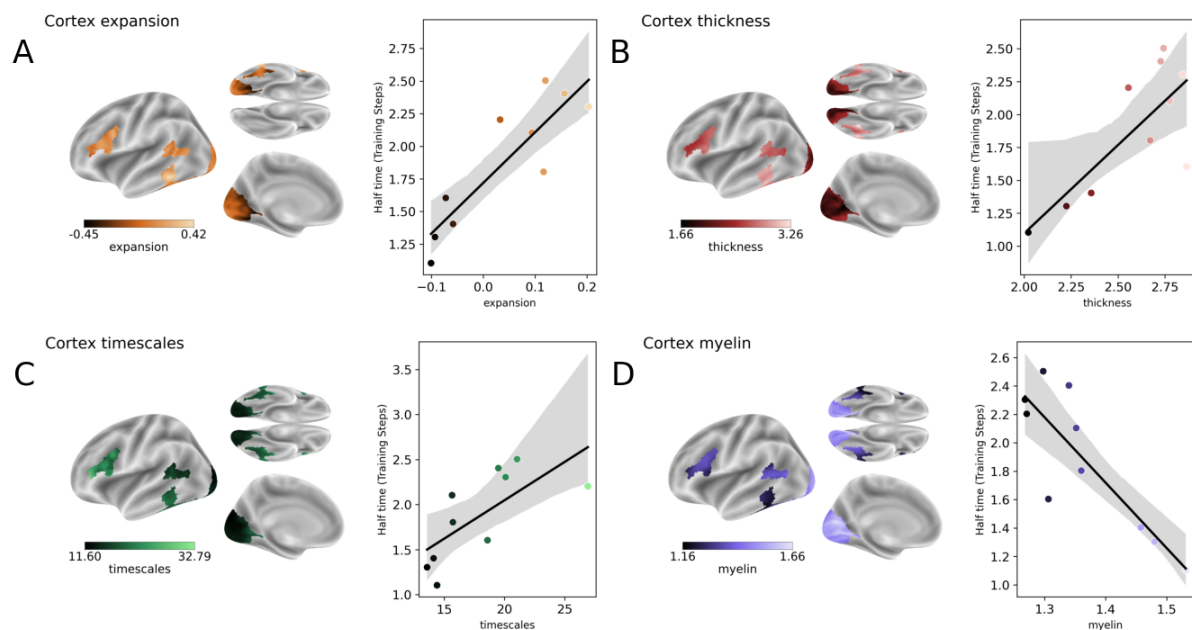
Figure 8 Relation between shared representations and cortical properties. **A.** Left. Cortical expansion index, as estimated from the difference between adults and infants' brains, for each ROI (Hill et al., 2010). Right. Correlation between cortical expansion and half time. Each dot is an ROI. **B.** Same as A for cortical thickness, as estimated from (Van Essen et al., 2013). **C.** Same as A for cortical time scales, as estimated from MEG source reconstruction in (Shafiei et al., 2021). **D.** Same as A for myelin concentration, as estimated from (Van Essen et al., 2013).

els rapidly acquire representations that align with the fast and low-level visual responses of the sensory cortices. In contrast, the emergence of slow and high-level representations – particularly those aligning with the prefrontal cortex – appears to require both far more training data.

This developmental trajectory echoes the biological development of the human cortex: the brain areas with which the AI models align last during their training are precisely those with the greatest cortical thickness, slower intrinsic timescales, prolonged maturation, and lower levels of myelination – i.e. the areas of the associative cortices that are known to slowly develop throughout the first two decades of life (Dehaene, 2021). This result suggests that the sequential acquisition of representations in artificial neural networks may spontaneously model some of the developmental trajectories of brain functions. In doing so, they may ultimately provide a new computational framework to understand the staged maturation of visual processing in biological systems (Vogelsang et al., 2024).

Open questions. Several results were not anticipated. First, the temporal score, encoding score and spatial score do not appear to emerge simultaneously – hence leading to the novel question of why these metrics follow this specific order. Second, the spatial and temporal scores are initially negative at the beginning of model training. This means that the deepest layers of a random DINOv3 tend to best predict fast and low-level brain responses at the very early (but not late) stages of training. Finally, the half times of these three metrics are reached in between 1% and 4% – i.e. only n=1.6B images – of DINOv3 training quantity. This suggests that while low-level brain-like representations are very quickly learnable, the high-level representations of the brain require a very large amount of data to be fully acquired.

Limitations. While this study offers a controlled analysis of brain–model convergence, several limitations warrant consideration. First, our findings are based exclusively on a single family of self-supervised vision models (DINOv3), which are hierarchical by design. It thus remains an open question whether similar spatial, temporal and encoding scores would emerge with other architectures and training objectives (Conwell et al., 2021). Second, fMRI and MEG offer limited resolution and thus provide coarse population-level brain activity and may overlook fine-grained neural mechanisms. Third, our analyses focus solely on the adult brain, leaving open the question of how these alignments emerge across development.

Understanding when these correspondences arise will require data from infants, children, or longitudinal cohorts (Evanson et al., 2025). Finally, while we quantify the similarity between representations from models and the brain, the exact nature and semantic structure of these neuronal representations continues to be a subject of intense ongoing research (Gifford et al., 2025; Graumann et al., 2022). Closing this interpretability gap certainly remains a major challenge to both neuroscience and AI.

Conclusion. Beyond the characterization of the spontaneous convergence between AI models and brains, these findings chart a path toward using AI models as tools to investigate the organizing principles of biological vision in the human brain. By showing how machines can come to see like us, our findings provide cues as to how the human brain may come to see the world.

References

Emily J. Allen, Ghislain St-Yves, Yihan Wu, Jesse L. Breedlove, Jacob S. Prince, Logan T. Dowdle, Matthias Nau, Brad Caron, Franco Pestilli, Ian Charest, J. Benjamin Hutchinson, Thomas Naselaris, and Kendrick Kay. A massive 7t fmri dataset to bridge cognitive neuroscience and artificial intelligence. *Nature Neuroscience*, 25(1):116–126, January 2022. ISSN 1546-1726. doi: 10.1038/s41593-021-00962-x. http://dx.doi.org/10.1038/s41593-021-00962-x.

Hubert Banville, Yohann Benchetrit, Stéphane d'Ascoli, Jérémy Rapin, and Jean-Rémi King. Scaling laws for decoding images from brain activity. *arXiv preprint arXiv:2501.15322*, 2025.

Francesco Cagnetta, Leonardo Petrini, Umberto M. Tomasini, Alessandro Favero, and Matthieu Wyart. How deep neural networks learn compositional data: The random hierarchy model. *Physical Review X*, 14 (3), July 2024. ISSN 2160-3308. doi: 10.1103/physrevx. 14.031001. http://dx.doi.org/10.1103/PhysRevX.14.031001.

Charlotte Caucheteux and Jean-Rémi King. Brains and algorithms partially converge in natural language processing. *Communications biology*, 5(1):134, 2022.

Bowen Cheng, Ishan Misra, Alexander G. Schwing, Alexander Kirillov, and Rohit Girdhar. Masked-attention mask transformer for universal image segmentation. 2022.

Radoslaw Martin Cichy, Aditya Khosla, Dimitrios Pantazis, Antonio Torralba, and Aude Oliva. Comparison of deep neural networks to spatio-temporal cortical dynamics of human visual object recognition reveals hierarchical correspondence. *Scientific Reports*, 6(1), June 2016. ISSN 2045-2322. doi: 10.1038/srep27755. http://dx.doi.org/10.1038/srep27755.

Colin Conwell, Jacob S. Prince, George A. Alvarez, and Talia Konkle. What can 5.17 billion regression fits tell us about artificial models of the human visual system? In *SVRHM 2021 Workshop @ NeurIPS*, 2021. https://openreview.net/forum?id=i_xiyGq6FNT.

Colin Conwell, Jacob S Prince, Kendrick N Kay, George A Alvarez, and Talia Konkle. What can 1.8 billion regressions tell us about the pressures shaping high-level visual representation in brains and machines? *BioRxiv*, pages 2022–03, 2022.

Stanislas Dehaene. *How we learn: Why brains learn better than any machine... for now.* Penguin, 2021.

Jia Deng, Wei Dong, Richard Socher, Li-Jia Li, Kai Li, and Li Fei-Fei. Imagenet: A large-scale hierarchical image database. In *2009 IEEE Conference on Computer Vision and Pattern Recognition*. IEEE, June 2009. doi: 10.1109/cvpr.2009.5206848. http://dx.doi.org/10.1109/CVPR.2009.5206848.

James J DiCarlo, Davide Zoccolan, and Nicole C Rust. How does the brain solve visual object recognition? *Neuron*, 73(3):415–434, 2012.

Adrien Doerig, Tim C. Kietzmann, Emily Allen, Yihan Wu, Thomas Naselaris, Kendrick Kay, and Ian Charest. High-level visual representations in the human brain are aligned with large language models. *Nature Machine Intelligence*, August 2025. ISSN 2522-5839. doi: 10.1038/s42256-025-01072-0. http://dx.doi.org/10.1038/s42256-025-01072-0.

Michael Eickenberg, Alexandre Gramfort, Gaël Varoquaux, and Bertrand Thirion. Seeing it all: Convolutional network layers map the function of the human visual system. *NeuroImage*, 152:184–194, 2017.

Andre Esteva, Brett Kuprel, Roberto A Novoa, Justin Ko, Susan M Swetter, Helen M Blau, and Sebastian Thrun. Dermatologist-level classification of skin cancer with deep neural networks. *nature*, 542(7639):115–118, 2017.

Linnea Evanson, Christine Bulteau, Mathilde Chipaux, Georg Dorfmüller, Sarah Ferrand-Sorbets, Emmanuel Raffo, Sarah Rosenberg, Pierre Bourdillon, and Jean-Rémi King. Emergence of language in the developing brain. Manuscript, May 2025. mailto:jeanremi@meta.com. Equal contribution by Pierre Bourdillon and Jean-Rémi King.

Daniel J Felleman and David C Van Essen. Distributed hierarchical processing in the primate cerebral cortex. *Cerebral cortex (New York, NY: 1991)*, 1(1):1–47, 1991.

Bruce Fischl. Freesurfer. *NeuroImage*, 62(2):774–781, August 2012. ISSN 1053-8119. doi: 10.1016/j.neuroimage. 2012.01.021. http://dx.doi.org/10.1016/j.neuroimage.2012.01.021.

Alessandro T. Gifford, Maya A. Jastrzębowska, Johannes J. D. Singer, and Radoslaw M. Cichy. In silico discovery of representational relationships across visual cortex. *Nature Human Behaviour*, June 2025. ISSN 2397-3374. doi: 10.1038/s41562-025-02252-z. http://dx.doi.org/10.1038/s41562-025-02252-z.

Alexandre Gramfort, Martin Luessi, Eric Larson, Denis A Engemann, Daniel Strohmeier, Christian Brodbeck, Roman Goj, Mainak Jas, Teon Brooks, Lauri Parkkonen, et al. Meg and eeg data analysis with mne-python. *Frontiers in Neuroinformatics*, 7:267, 2013.

Monika Graumann, Caterina Ciuffi, Kshitij Dwivedi, Gemma Roig, and Radoslaw M. Cichy. The spatiotemporal neural dynamics of object location representations in the human brain. *Nature Human Behaviour*, 6(6):796–811, February 2022. ISSN 2397-3374. doi: 10.1038/s41562-022-01302-0. http://dx.doi.org/10.1038/s41562-022-01302-0.

Uri Hasson, Samuel A. Nastase, and Ariel Goldstein. Direct fit to nature: An evolutionary perspective on biological and artificial neural networks. *Neuron*, 105

(3):416–434, February 2020. ISSN 0896-6273. doi: 10.1016/j.neuron.2019.12.002. http://dx.doi.org/10.1016/j.neuron.2019.12.002.

Martin N. Hebart, Oliver Contier, Lina Teichmann, Adam H. Rockter, Charles Zheng, Alexis Kidder, Anna Corriveau, Maryam Vaziri-Pashkam, and Chris I. Baker. "things-meg", 2023a.

Martin N Hebart, Oliver Contier, Lina Teichmann, Adam H Rockter, Charles Y Zheng, Alexis Kidder, Anna Corriveau, Maryam Vaziri-Pashkam, and Chris I Baker. THINGS-data, a multimodal collection of large-scale datasets for investigating object representations in human brain and behavior. *eLife*, 12:e82580, feb 2023b. ISSN 2050-084X. doi: 10.7554/eLife.82580. https://doi.org/10.7554/eLife.82580.

Jason Hill, Terrie Inder, Jeffrey Neil, Donna Dierker, John Harwell, and David Van Essen. Similar patterns of cortical expansion during human development and evolution. *Proceedings of the National Academy of Sciences*, 107(29):13135–13140, 2010.

Minyoung Huh, Brian Cheung, Tongzhou Wang, and Phillip Isola. The platonic representation hypothesis. *arXiv preprint arXiv:2405.07987*, 2024.

Jean-Rémi King and Stanislas Dehaene. Characterizing the dynamics of mental representations: the temporal generalization method. *Trends in cognitive sciences*, 18(4):203–210, 2014.

Nikolaus Kriegeskorte. Deep neural networks: A new framework for modeling biological vision and brain information processing. *Annual Review of Vision Science*, 1(1):417–446, November 2015. ISSN 2374-4650. doi: 10.1146/annurev-vision-082114-035447. http://dx.doi.org/10.1146/annurev-vision-082114-035447.

Nikolaus Kriegeskorte, Marieke Mur, and Peter A Bandettini. Representational similarity analysis-connecting the branches of systems neuroscience. *Frontiers in systems neuroscience*, 2:249, 2008.

Tom Dupré La Tour, Michael Eickenberg, Anwar O Nunez-Elizalde, and Jack L Gallant. Feature-space selection with banded ridge regression. *NeuroImage*, 264:119728, 2022.

Alice V. De Lorenci, Seung Eun Yi, Théo Moutakanni, Piotr Bojanowski, Camille Couprie, Juan C. Caicedo, and Wolfgang Maximilian Anton Pernice. Scaling channel-adaptive self-supervised learning. *Transactions on Machine Learning Research*, 2025. ISSN 2835-8856. https://openreview.net/forum?id=pT8sgtRVAf.

Florian P. Mahner, Lukas Muttenthaler, Umut Güçlü, and Martin N. Hebart. Dimensions underlying the representational alignment of deep neural networks with humans. *Nature Machine Intelligence*, 7(6): 848–859, June 2025. ISSN 2522-5839. doi: 10.1038/s42256-025-01041-7. http://dx.doi.org/10.1038/s42256-025-01041-7.

Ross D Markello, Justine Y Hansen, Zhen-Qi Liu, Vincent Bazinet, Golia Shafiei, Laura E Suárez, Nadia Blostein, Jakob Seidlitz, Sylvain Baillet, Theodore D Satterthwaite, et al. Neuromaps: structural and functional interpretation of brain maps. *Nature Methods*, 19(11): 1472–1479, 2022.

Johannes Mehrer, Courtney J. Spoerer, Nikolaus Kriegeskorte, and Tim C. Kietzmann. Individual differences among deep neural network models. *Nature Communications*, 11(1), November 2020. ISSN 2041-1723. doi: 10.1038/s41467-020-19632-w. http://dx.doi.org/10.1038/s41467-020-19632-w.

Juliette Millet, Charlotte Caucheteux, Pierre Orhan, Yves Boubenec, Alexandre Gramfort, Ewan Dunbar, Christophe Pallier, and Jean-Remi King. Toward a realistic model of speech processing in the brain with self-supervised learning, 2023. https://arxiv.org/abs/2206.01685.

Thomas Naselaris, Kendrick N Kay, Shinji Nishimoto, and Jack L Gallant. Encoding and decoding in fMRI. *Neuroimage*, 56(2):400–410, 2011.

Mitja Nikolaus, Milad Mozafari, Nicholas Asher, Leila Reddy, and Rufin VanRullen. Modality-agnostic fmri decoding of vision and language, 2024. https://arxiv.org/abs/2403.11771.

F. Pedregosa, G. Varoquaux, A. Gramfort, V. Michel, B. Thirion, O. Grisel, M. Blondel, P. Prettenhofer, R. Weiss, V. Dubourg, J. Vanderplas, A. Passos, D. Cournapeau, M. Brucher, M. Perrot, and E. Duchesnay. Scikit-learn: Machine learning in Python. *Journal of Machine Learning Research*, 12:2825–2830, 2011.

Niranjan Rajesh, Georgin Jacob, and SP Arun. Brain-like emergent properties in deep networks: impact of network architecture, datasets and training, 2024. https://arxiv.org/abs/2411.16326.

Joseph Redmon, Santosh Divvala, Ross Girshick, and Ali Farhadi. You only look once: Unified, real-time object detection, 2016. https://arxiv.org/abs/1506.02640.

Martin Schrimpf, Jonas Kubilius, Ha Hong, Najib J. Majaj, Rishi Rajalingham, Elias B. Issa, Kohitij Kar, Pouya Bashivan, Jonathan Prescott-Roy, Franziska Geiger, Kailyn Schmidt, Daniel L. K. Yamins, and James J. DiCarlo. Brain-score: Which artificial neural network for object recognition is most brain-like? September 2018. doi: 10.1101/407007. http://dx.doi.org/10.1101/407007.

K. Seeliger, M. Fritsche, U. Güçlü, S. Schoenmakers, J.-M. Schoffelen, S.E. Bosch, and M.A.J. van Gerven. Convolutional neural network-based encoding and decoding of visual object recognition in space and time. *NeuroImage*, 180:253–266, October 2018. ISSN 1053-8119. doi: 10.1016/j.neuroimage.2017.07.018. http://dx.doi.org/10.1016/j.neuroimage.2017.07.018.

Golia Shafiei, Sylvain Baillet, and Bratislav Misic. Human

electromagnetic and haemodynamic networks systematically converge in unimodal cortex and diverge in transmodal cortex. September 2021. doi: 10.1101/2021.09.07.458941. http://dx.doi.org/10.1101/2021.09.07.458941.

Guobin Shen, Dongcheng Zhao, Yiting Dong, Qian Zhang, and Yi Zeng. Alignment between brains and ai: Evidence for convergent evolution across modalities, scales and training trajectories, 2025. https://arxiv.org/abs/2507.01966.

Oriane Siméoni, Huy V. Vo, Maximilian Seitzer, Federico Baldassarre, Maxime Oquab, Cijo Jose, Vasil Khalidov, Marc Szafraniec, Seungeun Yi, Michaël Ramamonjisoa, Massa Francisco, Daniel Haziza, Luca Wehrstedt, Jianyuan Wang, Timothée Darcet, Théo Moutakanni, Leonel Sentana, Claire Roberts, Andrea Vedaldi, Jamie Tolan, John Brandt, Camille Couprie, Julien Mairal, Hervé Jégou, Patrick Labatut, and Piotr Bojanowski. Dinov3. *arXiv preprint arXiv:2025.00000*, 2025. TL;DR: DINOv3.

Katerina Marie Simkova, Adrien Doerig, Clayton Hickey, and Ian Charest. Representations in vision and language converge in a shared, multidimensional space of perceived similarities, 2025. https://arxiv.org/abs/2507.21871.

S.H. Solomon, K. Kay, and A.C. Schapiro. Semantic plasticity across timescales in the human brain. *bioRxiv*, 2024. doi: 10.1101/2024.02.07.579310. https://www.biorxiv.org/content/early/2024/05/24/2024.02.07.579310. Publisher: Cold Spring Harbor Laboratory.

Jerry Tang, Meng Du, Vy A. Vo, Vasudev Lal, and Alexander G. Huth. Brain encoding models based on multimodal transformers can transfer across language and vision, 2023. https://arxiv.org/abs/2305.12248.

Yingtian Tang, Abdulkadir Gokce, Khaled Jedoui Al-Karkari, Daniel Yamins, and Martin Schrimpf. Many-two-one: Diverse representations across visual pathways emerge from a single objective. July 2025. doi: 10.1101/2025.07.22.664908.

Imran Thobani, Javier Sagastuy-Brena, Aran Nayebi, Jacob S. Prince, Rosa Cao, and Daniel LK Yamins. Model-brain comparison using inter-animal transforms. In *8th Annual Conference on Cognitive Computational Neuroscience*, 2025. https://openreview.net/forum?id=bra729zCMm.

Michael Tschannen, Alexey Gritsenko, Xiao Wang, Muhammad Ferjad Naeem, Ibrahim Alabdulmohsin, Nikhil Parthasarathy, Talfan Evans, Lucas Beyer, Ye Xia, Basil Mustafa, Olivier Hénaff, Jeremiah Harmsen, Andreas Steiner, and Xiaohua Zhai. Siglip 2: Multilingual vision-language encoders with improved semantic understanding, localization, and dense features, 2025. https://arxiv.org/abs/2502.14786.

David C Van Essen, Stephen M Smith, Deanna M Barch, Timothy EJ Behrens, Essa Yacoub, Kamil Ugurbil, Wu-Minn HCP Consortium, et al. The wu-minn human connectome project: an overview. *Neuroimage*, 80: 62–79, 2013.

Loek van Rossem and Andrew M. Saxe. When representations align: Universality in representation learning dynamics, 2024. https://arxiv.org/abs/2402.09142.

Pauli Virtanen, Ralf Gommers, Travis E Oliphant, Matt Haberland, Tyler Reddy, David Cournapeau, Evgeni Burovski, Pearu Peterson, Warren Weckesser, Jonathan Bright, et al. Scipy 1.0: fundamental algorithms for scientific computing in python. *Nature methods*, 17(3): 261–272, 2020.

Lukas Vogelsang, Marin Vogelsang, Gordon Pipa, Sidney Diamond, and Pawan Sinha. Butterfly effects in perceptual development: A review of the 'adaptive initial degradation' hypothesis. *Developmental Review*, 71:101117, March 2024. ISSN 0273-2297. doi: 10.1016/j.dr.2024.101117.

Daniel L K Yamins and James J DiCarlo. Using goal-driven deep learning models to understand sensory cortex. *Nature Neuroscience*, 19(3):356–365, February 2016. ISSN 1546-1726. doi: 10.1038/nn.4244. http://dx.doi.org/10.1038/nn.4244.

Daniel L. K. Yamins, Ha Hong, Charles F. Cadieu, Ethan A. Solomon, Darren Seibert, and James J. DiCarlo. Performance-optimized hierarchical models predict neural responses in higher visual cortex. *Proceedings of the National Academy of Sciences*, 111 (23):8619–8624, May 2014a. ISSN 1091-6490. doi: 10.1073/pnas.1403112111. http://dx.doi.org/10.1073/pnas.1403112111.

Daniel LK Yamins, Ha Hong, Charles F Cadieu, Ethan A Solomon, Darren Seibert, and James J DiCarlo. Performance-optimized hierarchical models predict neural responses in higher visual cortex. *Proceedings of the national academy of sciences*, 111(23):8619–8624, 2014b.

Chengxu Zhuang, Siming Yan, Aran Nayebi, Martin Schrimpf, Michael C. Frank, James J. DiCarlo, and Daniel L. K. Yamins. Unsupervised neural network models of the ventral visual stream. *Proceedings of the National Academy of Sciences*, 118(3), January 2021. ISSN 1091-6490. doi: 10.1073/pnas.2014196118. http://dx.doi.org/10.1073/pnas.2014196118.